DOI: 10.13009/EUCASS2025-518
11TH EUROPEAN CONFERENCE FOR AERONAUTICS AND SPACE SCIENCES (EUCASS)

Numerical analysis on the influence of rotor configuration on quad-rotor flight performance

Luis Miguel García-Cuevas[⋆†]*, Jorge García-Tiscar*[⋆]*, Pau Varela*[⋆] *and Brendan Mullen*[⋆]
[⋆]*CMT – Clean Mobility & Thermofluids, Universitat Politècnica de València*
Camino de Vera s/n, 46022 Valencia, Spain
luiga12@mot.upv.es · jorgarti@mot.upv.es · pavamar@mot.upv.es · bmullen@upv.es
[†]Corresponding author

Abstract

The relatively low aerodynamic efficiency of quad-rotor UAVs in forward flight has motivated several investigations into the potential performance benefits of alternative rotor configurations. Some relevant works on the topic include numerical and experimental studies carried out by Patricia V. Diaz and Steven Yoon,[4] J. Tang and M. Mueller,[13] and David Langkamp,[7] which showed that the placement of the rotor and the tilt of the fixed rotor can be leveraged to help alleviate these limitations. Despite interest in the matter, an extensive Computational Fluid Dynamics study on the extent to which rotor configuration can enhance trimmed forward flight performance has yet to be undertaken. In addition to addressing this gap in the literature, the current work accomplishes its goal by applying a novel medium-fidelity CFD workflow that tackles two of the main limitations of existing studies: The employed approach automates the process of simulating quad-rotor trim through the coupling of a Proportional-Integral based algorithm and incorporates the rotors using the Actuator Disk Model, significantly increasing the practicality of such an approach thanks to its reduced computational cost.

1. Introduction

The use of Multi-rotor Unmanned Aerial Vehicles (UAVs) has seen significant uptake in the last decade. Their excellent manoeuvrability, Vertical take-off and Landing (VTOL) capability, and excellent stability have made them the aircraft of choice for a vast number of different missions such as from aerial photography and mapping, package delivery, and surveillance. Despite their numerous advantages, conventional multi-rotor systems still generally suffer from reduced endurance, range and top speed when compared to their fixed winged counterparts. For instance, DJI's latest commercial quad-rotor, the DJI Mavic Pro 4 has maximum rated endurance, range, and top speed of 51 minutes, 41 km, and 25 m/s respectively.[2] These metrics still fall short of those of fixed winged aircraft of similar size, such as the Delair UX11's 80 minutes maximum endurance, 53 km maximum range, and 54 m/s cruise speed.[1] The lower flight performance of conventional multi-rotor systems is in part tied to their necessity to tilt towards the direction of desired flight, in turn increasing their drag significantly. This inherent limitation has motivated several studies into the use of alternative rotor configurations in which the rotors are mounted at an angle relative to the airframe. Examples innovative designs resulting from the said studies are the QUaRTM and PairTilt tilting quad-rotors designed by M.Mueller and J.Tang,[12,13] and the lifting body tilt quad-rotor designed by H.Zhang et al.[14] Despite the existing research effort, an extensive study aiming at quantifying the effects of tilting the rotors is yet to be performed. The current work addresses this gap in the literature by evaluating the performance of several tilted rotor UAV configurations, including a modified configuration in which vertical separation is introduced between the arms in order to compensate some of the potential drawbacks of tilted rotors. The study is carried out using a novel and novel steady-state Computational Fluid Dynamics approach proposed in a yet unpublished study by L.M. Garcia-Cuevas et al.[5] that couples a P-I based trim algorithm to simulate the quad-rotor in trimmed flight conditions. The document is structured as follows: First, Section 2 describes the quad-rotor UAV chosen for the analysis. Following this, the computational resources used for the numerical analysis are provided in Section 3. Next, a preliminary analysis is carried out in Section 4 to determine the potential benefits of different configurations and inform the designs that are evaluated through CFD simulations. Subsequently, the simulation campaign is summarised in Section 5 and the simulation approach and methodology is covered in Section 6. Thereafter, the simulation results and computational cost are presented and discussed in Sections 7 and 8. Finally, concluding remarks are presented in Section 9.

DOI: 10.13009/EUCASS2025-518

2. Case study

The current work evaluates the forward flight performance of several designs based on the PairTilt quad-rotor UAV designed and manufactured by J. Tang and M.Mueller[13] from the Department of Mechanical Engineering of the Berkeley University of California. A three-dimensional render of the original assembly is shown in Figure 1. The PairTilt UAV differs from traditional quad-rotor systems as it is able to independently tilt the front and back arms to which the rotors are mounted to through the use of servos, allowing for thrust vectoring in the UAV's symmetry plane and actuation along five degrees of freedom. The UAV is 330 mm long, 306 mm wide, and 60 mm tall when laid flat. The UAV's length is used as its characteristic length L_{UAV} in the current work. In its non-tilted configuration, the rotors are separated by a distance of 220 mm along the x-direction and 276 mm along the y-direction. The PairTilt's has a mass (m_{UAV}) of 1000 g or 965 g depending on whether the tilting mechanism mounted. As assumed by J. Tang and M.Mueller,[13] the aircraft's Centre of Gravity (CoG) is considered to be located at the centre point of the front and back arms. The UAV's reference area A is equal to 0.05 m^2. The original design is equipped with four commercially available 8 inch 8045 ABS rotors.

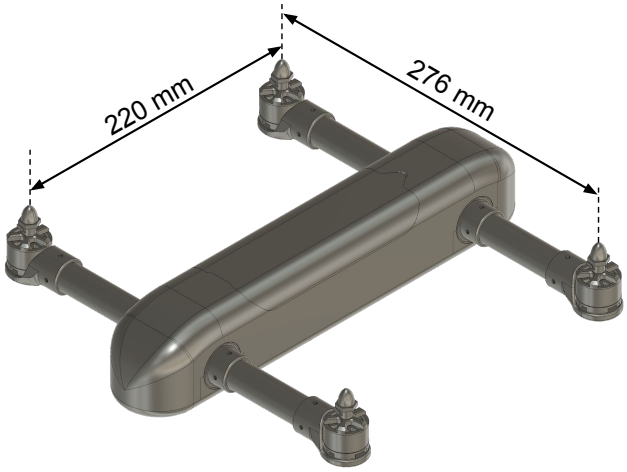

Figure 1: Three-dimensional render of the original PairTilt quad-rotor UAV assembly designed and manufactured by J. Tang and M.Mueller.[13]

The PairTilt quad-rotor was elected as a baseline platform for the analysis carried in this work for several reasons. Firstly, the original aircraft was designed such that the rotors can be tilted by a wide rage of angles. Secondly, experimental flight test data was made available by its authors, allowing for a comparison with the obtained numerical results. Finally, its relatively simple geometry makes it an ideal candidate for rapid design modifications through the use of 3-D modelling software.

3. Computational resources and software

All CFD simulations in the current work are carried out using the Simcenter STAR-CCM+ commercial software,[11] and are computed using 778 cores on seven of the Universitat Politecnica de Valencia's (UPV) Sirius Scientific Computing Cluster's[3] nodes equipped with 2× Intel Xeon 8480 CPUs each.

4. Theory and preliminary analysis

To obtain an initial understanding of the effects of tilting the rotors on a small scale quad-rotor system's forward flight performance, and inform the designs chosen for the parametric analysis carried out through CFD simulations, a preliminary analysis is carried out using flight mechanics principles.

4.1 Identifying the potential benefits of a tilted rotor configuration

To begin, two reference frames are defined. The first is the local horizon frame denoted $\mathfrak{R}_h$, and its axes are denoted x^h, y^h, and z^h. The frame is centred on the UAV's Center of Gravity (CoG) and its orientation is fixed relative to earth such that the UAV's weight (W) acts along the z^h direction. Moreover, the UAV's direction of travel through a static

DOI: 10.13009/EUCASS2025-518

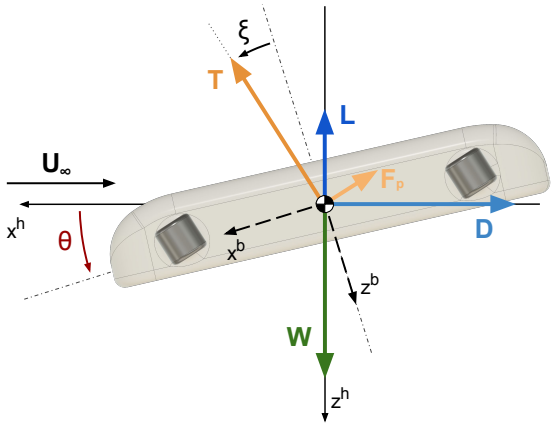

Figure 2: Schematic diagram representing the different forces acting on the UAV in its tilted rotor configuration while in non-accelerated forward flight conditions.

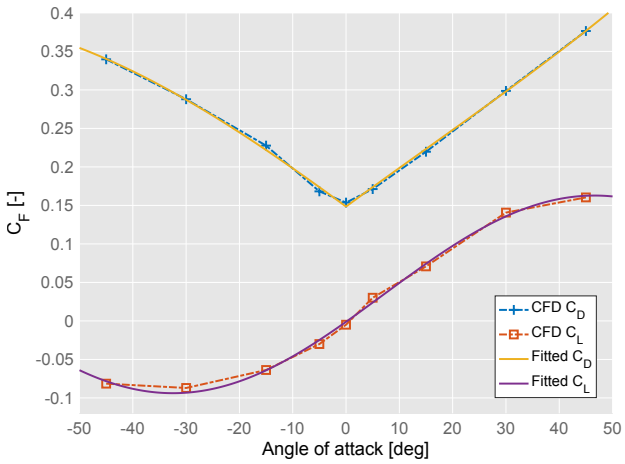

Figure 3: Comparison between the aerodynamic coefficients of the PairTilt airframe obtained through CFD and their fitted curves.

atmosphere is defined along x^h. Next a body frame denoted $\mathfrak{R}_b$ and tied to the UAV's airframe is defined, such that its x^b-axis is the reference line. The frame is also centred on the CoG, and its other axes are also marked with a ^{b} subscript. Since the analysis is constrained to forward and levelled flight conditions, an assumption of symmetry is made. All forces perpendicular to, and all moments parallel to the UAV's symmetry plane are therefore considered null throughout this work. Moreover, the UAV's roll and yaw angles are considered null. Only the pitch angle (θ) accounted for. Where θ defines the UAV's orientation relative to $\mathfrak{R}_h$ and is measured about y^b, in other words a negative pitch angles means the UAV's nose is pointing down. The forces acting on the UAV while in non accelerated forward flight conditions can thus be reduced to: the airframe's aerodynamic drag (D) and aerodynamic lift (L), the UAV's weight (W), the total thrust generated by the rotors (T), and tangential rotor forces (F_p). Figure 2 illustrates the aforementioned forces where U_∞ is the air's relative velocity. The scenario corresponds to a case in which all four of the UAV's rotors are tilted by the same angle denoted ξ. The tilt angle is defined relative to the body frame and is considered positive when the rotors are tilted forward (rotated about -y^b). For the sake of simplicity, the tangential forces on the rotors are neglected in this preliminary analysis, and the vertical and horizontal components of the sum of forces acting on the UAV can be written as:

$$\sum F_{z^h} = -T \cdot \cos(\theta - \xi) + W - L, \tag{1}$$

and

$$\sum F_{x^h} = -T \cdot \sin(\theta - \xi) - D, \tag{2}$$

respectively. Since Equations 1 and 2 are null in trimmed conditions and the following relationship can be established:

$$\theta = -\arctan\left(\frac{D}{W - L}\right) + \xi, \tag{3}$$

where $(\xi - 90°) < \theta \leq \xi$. Next, the isolated airframe's drag and lift coefficients are computed using CFD for different pitch angles at an airspeed of 20 m/s, and are fitted with the following functions:

$$C_D = a\theta^3 + b\theta^2 + c|\theta| + d, \tag{4}$$

$$C_L = a_0 + a_1 \cdot \cos(\theta \cdot w) + b_1 \cdot \sin(\theta \cdot w). \tag{5}$$

Equations 4 and 5 are plotted against the CFD data in Figure 3. The comparison shows that the functions are a good fit for the desired range of angles of attack and for the purpose of this initial analysis. The coefficients of the fitted functions are provided in Appendix B, for θ expressed in degrees. Equations 4 and 5 are then used to determine L and D as a function of the angle of attack on the airframe for a given airspeed V using the following relationship:

$$F = \frac{1}{2} A \cdot \rho \cdot V^2 \cdot C_F, \tag{6}$$

DOI: 10.13009/EUCASS2025-518

where F is either the Drag or Lift force, C_F is the corresponding force coefficient, A is the airframe's reference area, and ρ is the density of air. For the sake of simplicity the aerodynamic coefficients are assumed to be independent of airspeed. A solution for Equation 3 is then numerically approximated by searching for the pitch angle that satisfies the equation. The step can then be repeated for a range of tilt angles and airspeeds. Once the trimmed pitch angle is known for each case, the trimmed lift, drag and total thrust forces can be extracted. The total thrust requirement is obtained using Equation 7 once drag and lift forces are computed.

$$T = \left[(W - L)^2 + D^2\right]^{1/2} \tag{7}$$

Finally, momentum theory is used to estimate the total mechanical power of the UAV, for which the steps are provided in Appendix A. Through the aforementioned steps, a first look at the effects of introducing different collective rotor tilt angles on the UAV's trimmed forward flight performance can be obtained. Figure 4 reports the evolution of the trimmed pitch angle, total thrust requirement, and total mechanical power for hover and forward flight up to an airspeed of 25 m/s for different rotor tilt angles, while Figure 5 reports the aerodynamic lift and drag forces on the airframe and the quad-rotor's Specific Range computed as: SR = 3.6 (Airspeed/Power) [km/Wh]. The results are computed using a mass $m_{\text{UAV}} = 1$ kg.

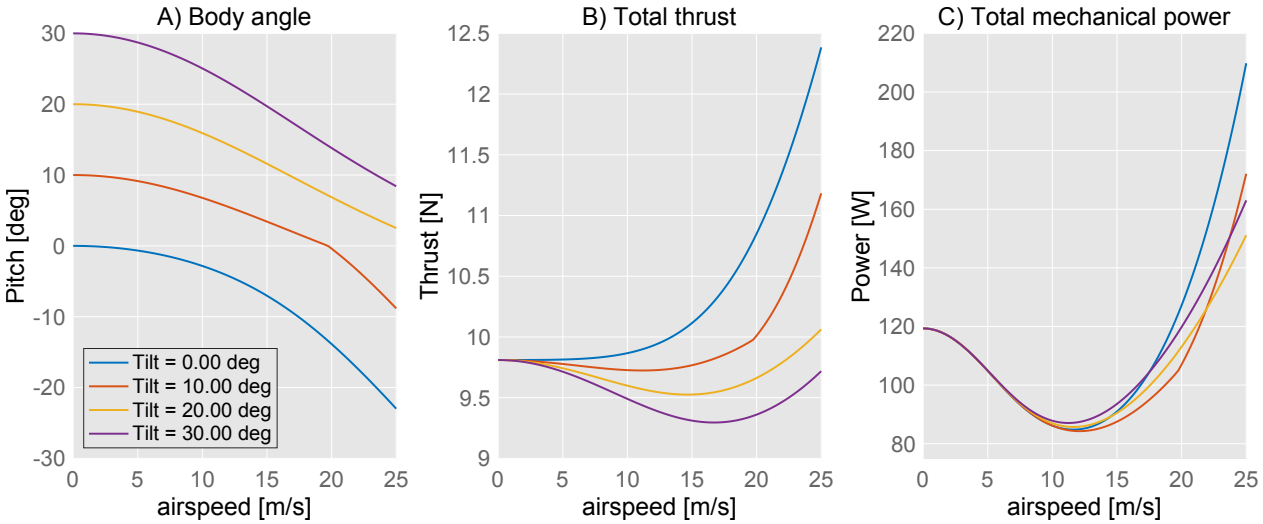

Figure 4: Initial prediction of the UAV's pitch angle, total thrust, and total mechanical power in trimmed forward flight conditions for different rotor tilt angles.

The preliminary results reveal several key trends. Firstly and in line with expectations, tilting the rotors forward causes the UAV's nose to point up in hover and generally increases the UAV's pitch angle. Secondly, increasing the rotors' tilt by $\Delta\xi$ does not necessarily increase the pitch angle by the same amount. In fact, the pitch angle difference between cases varies quite significantly with airspeed, and is tied to the non-linear and coupled nature of Equation 3, describing the relationship between the forces acting on the UAV and its trimmed pitch angle. Moreover, it can be seen that the largest tilt angles bring about the smallest relative difference in pitch. The latter can be explained by the fact that the said cases maintain a positive and relatively large pitch angle even at moderate airspeeds, resulting in increased aerodynamic forces on the airframe, therefore requiring more horizontal thrust and a slightly reduced pitch angle relative to what would be expected otherwise. Crucially, the findings of this first analysis align with the hypothesis that tilting the rotors can benefit multi-rotor performance in forward flight, as illustrated by the reduced power and increased Specific Range for some non-zero tilt angles, observed in Figures 4C, and Figure 5C respectively. However the preliminary analysis also suggests that the lowest power, and therefore the highest endurance is not achieved by the case with the largest tilt angle, but by an intermediate one. A similar trend is observed when comparing the cases' specific range. As mentioned in the previous paragraph, the cases with the highest tilt angles suffer from increased aerodynamic forces at low to moderate airspeeds, and therefore only present a reduced total power at the highest airspeeds when compared to the non-tilted and $\xi = 10°$ cases, implying that very large tilt angles would mainly provide a benefit in terms of increasing the UAV's maximum speed.

DOI: 10.13009/EUCASS2025-518

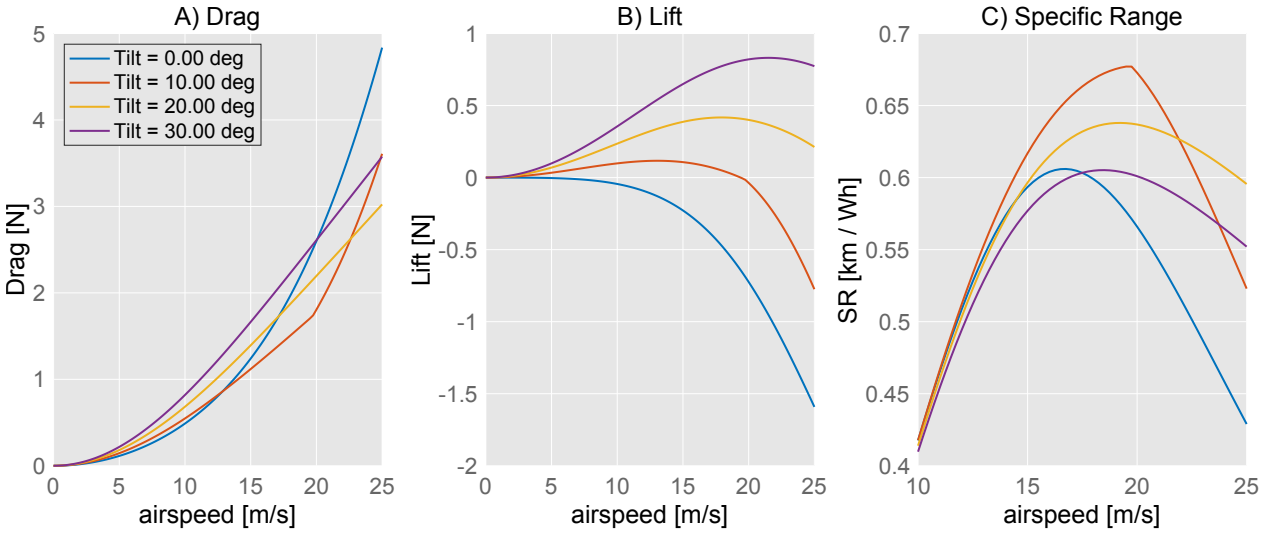

Figure 5: Initial prediction of airframe drag and lift forces, and the UAV's Specific Range in trimmed forward flight conditions for different rotor tilt angles.

4.2 Identifying the drawbacks of a tilted rotor configuration

Despite the potential power savings benefits identified in the previous section, there are several drawbacks to introducing a rotor tilt. The first of these drawbacks is the reduced pitching authority. In an non-tilted configuration, a given thrust differential $\Delta T = T_f - T_b$ between the front and back rotors allows the UAV to generate a pitching moment equal to $M_y = l_1 \Delta T/2$, where T_f and T_b are the thrust generated by the fore and aft rotor pairs respectively, and l_1 is the distance separating the rotors along the x-direction. This scenario is illustrated in in Figure 6.

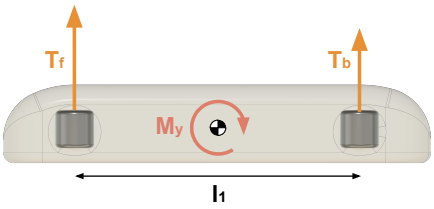

Figure 6: Schematic diagram illustrating the pitching moment generated by the thrust differential between the front and back rotors in an non-tilted configuration.

In a tilted configuration, the distance between the rotors' axes of rotation and their thrust vectors becomes $l_2 = \cos(\xi) \cdot l_1$ as illustrated in Figure 7(a), and the UAV's pitching authority is reduced by the same factor. For instance, a tilt angle of 30° reduces the UAV's pitch authority by 23.3 %. The effect is highly undesirable as it could negatively impact the UAV's agility when performing manoeuvrers, increase the angular rate and thrust differential between rotors, and potentially limit the aircraft's flight envelope due to an earlier onset of pitch saturation. In addition to reducing the UAV's pitch authority, the decreased lateral separation between the rotors in a tilted configuration can lead to significant overlap between rotors while in forward flight, causing the back rotors to operate in the wake of the front rotors and negatively affecting their efficiency. To minimize both of the aforementioned drawbacks, the back arms and rotors can be placed higher than the front arms without significantly affecting the UAV's physical footprint, as illustrated in Figure 7(b) where the vertical offset between the rotors is denoted dz. For the sake of simplicity, the angle that the line connecting the front and aft rotors' origin makes with the airframe's reference line is denoted $\chi = \arctan(dz/l_1)$. In this offset rotor configuration the distance between the front and back rotors' thrust vectors becomes $l_3 = l_1 \cdot \cos(\xi - \chi)/\cos(\chi)$. If dz is selected such that $\chi = \xi/2$, the original loss in pitching authority induced by tilting the rotors is completely negated while maintaining a tilt angle of ξ. For instance, a case in which the rotors are tilted by 40° would only require a vertical offset (dz) equal to 36.4% of the original distance separating the rotors (l_1) in order to re-establish the pitching authority of a non-tilted configuration.

DOI: 10.13009/EUCASS2025-518

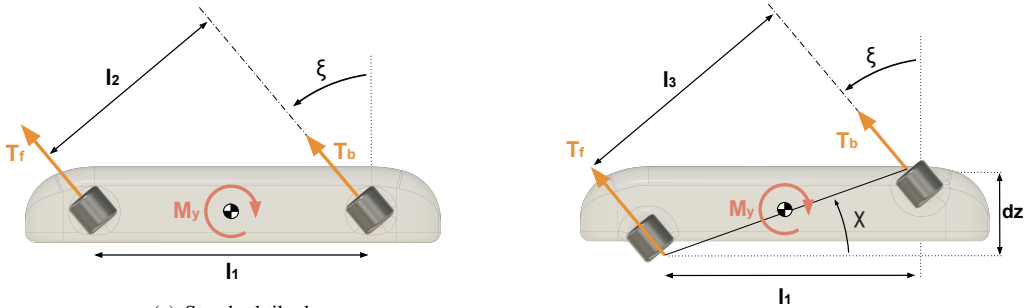

(a) Standard tilted (b) Offset tilted

Figure 7: Schematic diagrams illustrating the pitching moment generated by the thrust differential between the front and back rotors in a tilted (a) and tilted offset (b) configuration.

5. Simulation campaign

Based on the preliminary analysis carried out in the previous section, three distinct configurations are evaluated using CFD. These configurations are shown in Figure 8, where the rotors are represented by dark grey disks. The first is the standard non-tilted configuration (a), which serves as the baseline case. The standard case's performance is evaluated for a mass of 1 kg and 965 g, which correspond to the PairTilt's mass with and without the tilting mechanism respectively. Following this, the UAV is simulated with tilt angles (b) of 10°, 20°, 30°, and 40°. Finally, an offset configuration (c) in which $\chi = 20°$ ($dz = 0.364 l_1$) is evaluated for tilt angles of 20°, 30°, and 40°.

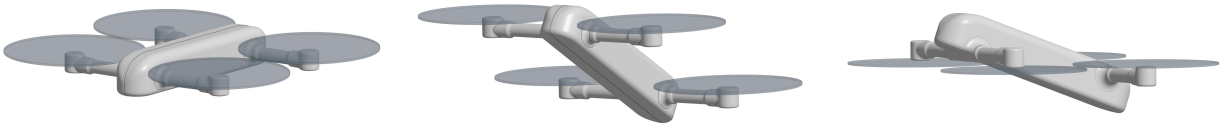

(a) Standard non-tilted configuration (b) Standard tilted configuration (c) Offset tilted configuration

Figure 8: A series of images depicting the three types of rotor configurations evaluated in the current work.

To help achieve the desired vertical separation between rotors without significantly increasing the physical extent of the UAV in the offset case, the front rotors are mounted in a pusher configuration below the front arms as shown in Figure 8(c). All configurations are simulated in trimmed forward and levelled flight conditions for airspeeds ranging between 2 m/s and 26 m/s at an interval of 2 m/s.

6. Methodology

6.1 General approach

The simulations are carried out in the UAV's body frame. At the start of each simulation a freestream velocity at the boundary is imposed such that it corresponds to the desired airspeed (V_{UAV}). The aerodynamic forces and moments predicted by the CFD solver are then used to compute three balance equations which the trim algorithm used to determine the set of control variables that satisfies a trimmed state through an equal number of feedback loops. The two first balance equations correspond to Equations 1 and 2 with an added term for the tangential rotor forces. The third balance equation corresponds to the sum of pitching moments on the UAV's Center of Gravity, and takes into account all moments on the airframe and those induced by the rotors. The CFD solver and trim algorithm exchange the aerodynamic loads and commands at each solver iteration until the simulation converges and a trimmed state is reached. The trim algorithm acts on the UAV's pitch angle, and the front and back rotors' angular rates (ω_1 and ω_2). The angular rate differential between the port and starboard rotors is considered null because of the assumption of symmetry.

DOI: 10.13009/EUCASS2025-518

6.2 Trimming algorithm

The trim algorithm is a simplified version of the one proposed by L.M Garcia-Cuevas et al.[5] The number of degrees of freedom and control variables is reduced to three in this implementation. A block diagram detailing its workings and its coupling to the CFD solver is presented in Figure 9(a). The algorithm combines a total of three Proportional-Integral (P-I) loops that each act on one the UAV's control variables at every CFD solver iteration (j) following equation 8:

$$u(j+1) = K_P \epsilon(j) + K_I \left(\sum_{k=0}^{j} \epsilon(k) \right), \tag{8}$$

where u is a control variable, K_P, and K_I are the proportional and integral coefficients respectively, and ϵ is the error of the associated balance equation. Since the algorithm's purpose consists in determining the combination of control variables that satisfies a trimmed state for a given airspeed and trajectory rather than replicating realistic quad-rotor flight dynamics, θ is explicitly controlled by P-I loops 2 tasked with trimming the forward components of the sum of forces. P-I loop 1 varies the collective angular rate of all rotors to regulate the total thrust magnitude and trim the vertical sum of forces. Finally, P-I number 3 adjusts the angular rate differentials between the front and back rotors in order to generate the thrust differential required to trim the aerodynamic pitching moments on the UAV's airframe and rotors. The contributions of P-I loops 1 and 3 are summed or subtracted depending on the the rotor. The rotor angular rates are constrained to positive values. The P-I loops were tuned by trial and error, and their coefficients are provided in Appendix **??**.

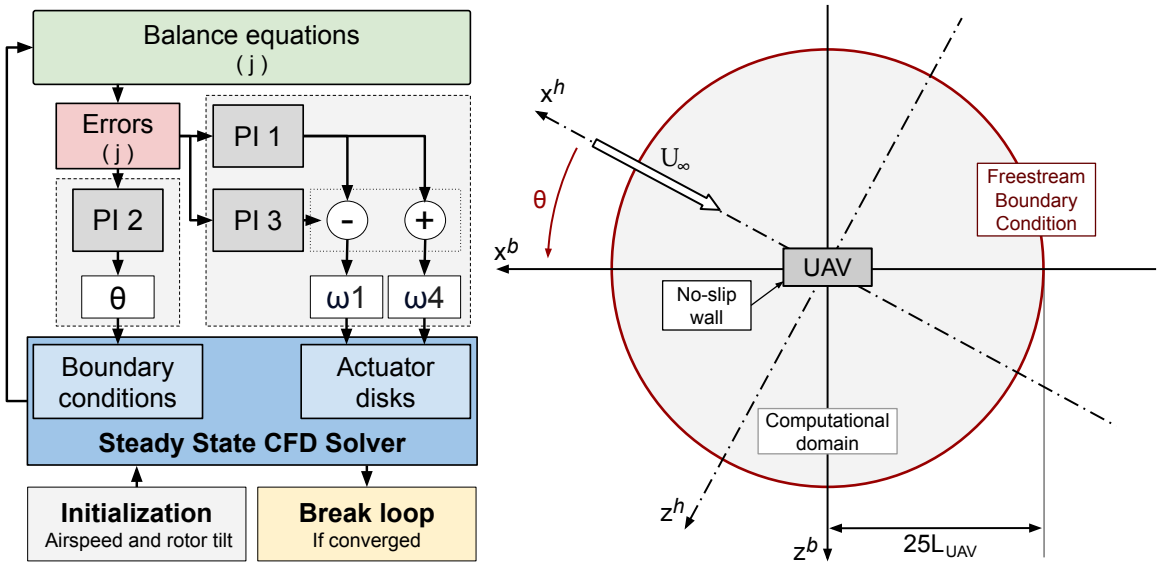

(a) Trim algorithm

(b) Computational domain and boundaries

Figure 9: (a) Block diagram of the trim algorithm and its coupling to the steady-state CFD solver, and (b) Schematic diagram of the computational domain and its boundaries. The diagram additionally highlights the manner in which the UAV's orientation and direction of travel are tracked and incorporated into the simulation. In this particular example $\theta < 0$.

6.3 Computational Fluid Dynamics set-up

6.3.1 Computational domain and boundary conditions

As shown in Figure 10(a), a hemisphere is selected as the computational domain. The domain is centred on the UAV and is given a radius of $25L_{\text{UAV}}$. A symmetry boundary condition is imposed at the domain's flat surface, and only half of the UAV is included in the domain. The UAV's airframe is defined as a no-slip wall while the domain's remaining outer surface is set as a free-stream boundary condition. Turbulence intensity and viscosity ratio of 1% and 10 are imposed at the free-stream, while the incident flow's temperature is set to 25 °C and its pressure to that at sea level. The free-stream velocity magnitude (U_∞) is set to the UAV's airspeed V_{UAV}, and its direction is defined along $-x_h$. Since

DOI: 10.13009/EUCASS2025-518

the simulation is carried out in $\mathfrak{R}_b$, the incident flow direction at the boundary evolves as the trim algorithm determines the correct vehicle attitude. A schematic diagram of the computational domain, the selected boundary conditions, and the manner in which the incident flow direction is varied based on the UAV's pitch angle is shown in Figure 9(b).

6.4 Solvers and Physical models

The simulations are carried out using a steady state Reynolds Averaged Navier-Stokes (RANS) approach. Turbulence is modelled using the Menter K-Omega SST linear eddy viscosity model.[9] The air is treated as an ideal gas and a implicit-coupled flow solver is used. As it was found that the airframe has the tendency to induce instabilities due to vortex shedding at certain airspeeds, a maximum Courant–Friedrichs–Levy (CFL) condition of 200 is used for the pseudo-time-marching solver, and a line search method is used to allow the solver to automatically select the solver's relaxation factor between 0.05 to 0.3. Additionally, a Continuity Convergence Accelerator with an under-relaxation factor of 0.01 is used.

6.5 Rotor modeling

The rotors are modelled using the Actuator Disk Model (ADM), which is referred to as the *Time-Averaged Virtual Disk Model* in Star-CCM+. This rotor modelling approach is advantageous as it includes the rotors effects on the flow field as momentum sources, and simulates the averaged effect of the rotor over its full rotation despite the steady state approach. In the current work, the Blade Element Method (BEM) sub-model is used to compute the strength of the source terms. The sub-model requires a look-up table describing the rotor's twist and chord distribution and a look-up table containing the aerodynamic characteristics of the rotor blade's airfoil for different angles of attack and Reynolds numbers. As an accurate 3-D model of the PairTilt rotors is not available, a twist and chord distribution for a near identical 8045 rotor is obtained from Derya Kaya's PhD. thesis,[6] and the T-MOTOR MS1101 rotor blade's airfoil polar is used for the aerodynamic look-up table. The ADM's azimuthal resolution is set to 38 while its radial resolution is set to 24 with a span-wise stretch factor of 0.95.

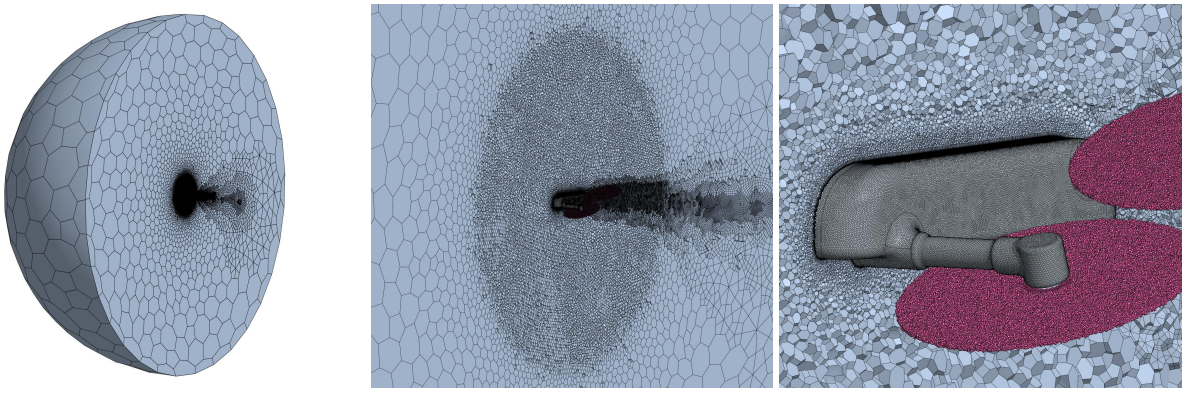

(a) Computational domain (b) Near-field and wake (c) Surface and actuator disks

Figure 10: Several representations of the computational domain's discretization.

6.5.1 Meshing

The computational domain is discretized using a hybrid polyhedral-prism mesh, with a low wall y^+ (<1.0) approach selected for the boundary layer modelling. Several representations of the domain's discretization are shown in Figure 10. A cell size of 2 m is used in the far field, while total of 20 prism cell layers are imposed near the UAV's walls. The total prism layer thickness is set to 2.5 mm. The airframe's geometry is discretized using a surface cell size of 0.8 mm ensuring adequate representation of the airframe's geometry and good cell aspect ratio and volume growth rate values at the wall and transition between prism and polyhedral cells respectively. A volumetric refinement is imposed in the near field and at the actuator disks such that the cell size in these regions is reduced to 20 mm and 1.5 mm respectively. Adaptive Mesh Refinement (AMR) is used to refine the cells in the UAV's wake. The mesh is refined for cells in which the flow's vorticity magnitude exceeds $100\,s^{-1}$ up to a minimum cell size of 4 mm. The aforementioned meshing parameters were selected based on a mesh sensitivity analysis and result in an average final cell count of 8×10^6.

DOI: 10.13009/EUCASS2025-518

6.5.2 Convergence criteria

Each CFD simulation is iterated until the UAV's total mechanical power, cell count in the domain, and aerodynamic force coefficients of the airframe vary by less than 0.5%, 1% and 1.0×10^{-3} respectively, over the course of 500 solver iterations. If the solver does not reach the aforementioned convergence criteria within 4000 iterations, the simulation is stopped and the results are discarded.

7. Results and discussion

7.1 Comparison with experimental data

To begin, the experimental measurements of the PaitTilt UAV's electrical power consumption published by J. Tang and M.Mueller[13] are compared with the numerical predictions in Figure 11.The electrical power of required for each rotor (P_e) is computed based on the simulation results using the following equation:

$$P_e = V_{\text{applied}} \cdot \left(\frac{Q}{K_t} + I_0 \right), \tag{9}$$

where V_{applied} is the estimated voltage applied to the motors, computed as:

$$V_{\text{applied}} = -\left((-103400 \cdot R_{\text{idle}} \cdot k_t \cdot Q^2 - 4 \cdot \Omega \cdot k_t \cdot Q + 1)^{1/2} - 1) \right) / (320 \cdot Q \cdot k_t). \tag{10}$$

and where R_{idle} is the motor's resistance, k_t is a temperature compensation factor, Q is rotor torque, Ω is the rotor's angular rate, K_t is the motor torque constant, and I_0 is the motor's inherent resistance load. The total electrical power of the UAV is then obtained by summing the four rotors' power are summed to that of the onboard electronics: $P_{\text{elec}} = V.I_{\text{idle}}$ where V is the battery pack's nominal voltage, and I_{idle} is the current drawn by the onboard electronics. Equations 9 and 10 were provided by J. Tang and M.Mueller,[13] and the values used for the aforementioned parameters are provided in Appendix B.

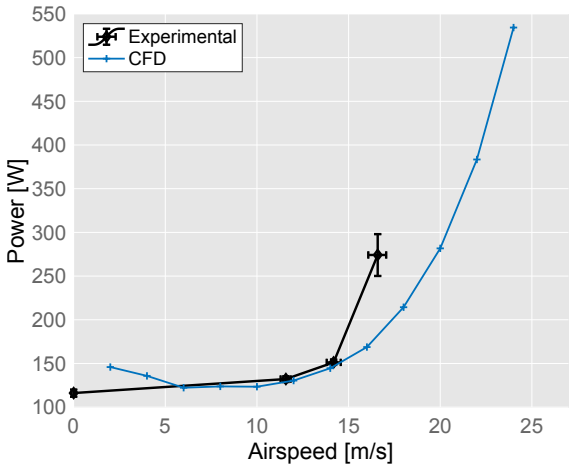

Figure 11: Comparison between the experimental and numerical prediction of the UAV's electrical power consumption in its standard configuration without the tilting mechanism ($m_{\text{UAV}} = 965$ g).

Figure 11 shows that the simulation approach captures the trend observed in the experimental data, and correctly predicts the UAV's electrical power for moderate airspeeds. However, a significant discrepancy in the results can be observed at very low and very high airspeeds. The under-predicted power at high airspeeds suggests that the aerodynamic forces acting on the airframe are under-predicted in the simulations, and could potentially be attributed to the simplified geometry used for in the CFD analysis. The over-predicted power at low speeds might suggests either an inadequate approximation of the rotor's aerodynamic performance by the ADM or an over-prediction of the effects of rotor downwash in the simulations, or a combination of both. Further investigation is required to identify the factors behind the observed discrepancies.

DOI: 10.13009/EUCASS2025-518

7.2 Evaluating the performance of the standard configuration with different tilt angles

In this section, the standard configuration's forward flight performance for different tilt angles is evaluated. From here on forward, all presented results correspond to the case in which the UAV's mass is equal to 1000 g. Figure 12 reports the different cases' pitch angle (a), total thrust requirements (b), and total mechanical power (c), while Figure 13 reports the aerodynamic forces on the airframe (a & b) and the configurations' Specific Range (c). The simulation results closely follow the trends predicted in the preliminary analysis. However significant differences in the values taken by the results can be noted. Generally speaking, the UAV pitch presents a much steeper downward slope as airspeed increases when compared to what was seen in Figure4(a). The latter is linked to the larger aerodynamic forces on the airframe predicted by the simulations and indicates that the presence of the rotors has a significant effect on the airframe's aerodynamic behaviour. If fact, unlike in the preliminary analysis, a noticeable initial increase in positive airframe lift is observed between 2 m/s and 6 m/s for all tilt angles here. Next, it can be seen that the UAV's minimum power is not significantly affected by changing the rotor tilt, as only a maximum difference of 2.3 W is observed between cases. Remarkably, the lowest power of all the evaluated cases is 87.3 W and was achieved by the non-tilted configuration at an airspeed of 8 m/s. The result suggests that wake interactions between rotors might be limiting the benefits of tilting the rotors. However, the difference in power is significantly more pronounced at the lowest and highest airspeeds. At the largest simulated airspeed of 26 m/s, the total mechanical power of the UAV is reduced by up to 37% with a tilt angle of 50°, while the tilted cases generally present higher power at the lowest airspeeds. Finally and in line with the preliminary analysis' findings, the simulation results also indicate that the highest Specific Range is not achieved by the case in which the rotors are tilted by the largest angle. Here, a tilt angle of $\xi = 30°$ was found to provide the best SR when compared to the rest of the case, with a maximum of 0.546 km/Wh at an airspeed of 18 m/s, which is a 10.2% increase compared to the non-tilted configuration's maximum of 0.495 km/Wh.

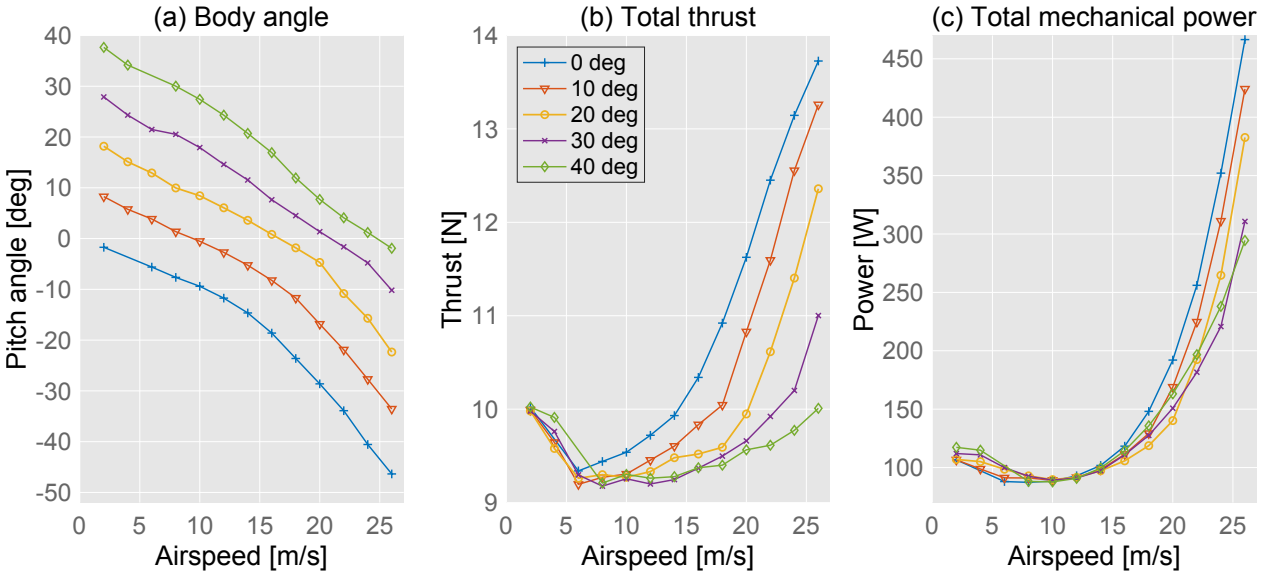

Figure 12: Comparison of the UAV's pitch angle (a), total thrust (b) and total mechanical power (c) in trimmed forward flight conditions for different rotor tilt angles.

Only two simulations did not reach the established convergence criteria, their results were therefore not reported.

7.3 Evaluating the performance benefits of introducing a vertical offset between the rotors for different tilt angles

Finally, the effect of introducing a vertical offset between the front and back rotors on the UAV's total mechanical power and Specific Range is evaluated for three different tilt angles. Figure 14 compares the power, while Figure 15 compares the SR for tilt angles of 20° (a), 30° (b), and 40° (c). The results show that the offset affects the cases differently. On one hand, the UAV's minimum power is reduced by 5.5% and 4% for tilt angles of 20° and 30° but is increased by 4.6% for the 40° case. On the other hand, the UAV's SR is mainly enhanced for the cases with the largest tilt angles, with the 30° and 40° cases benefiting from a significant 15.9% and 12.1% increase in maximum SR respectively, compared to the small increase of only 1.89% observed for the $\xi = 20°$ case. The vertical separation between rotors likely provides the highest benefit when $\xi = 30°$ due to the fact that the $\xi = 20°$ case does not suffer from rotor wake interactions even

DOI: 10.13009/EUCASS2025-518

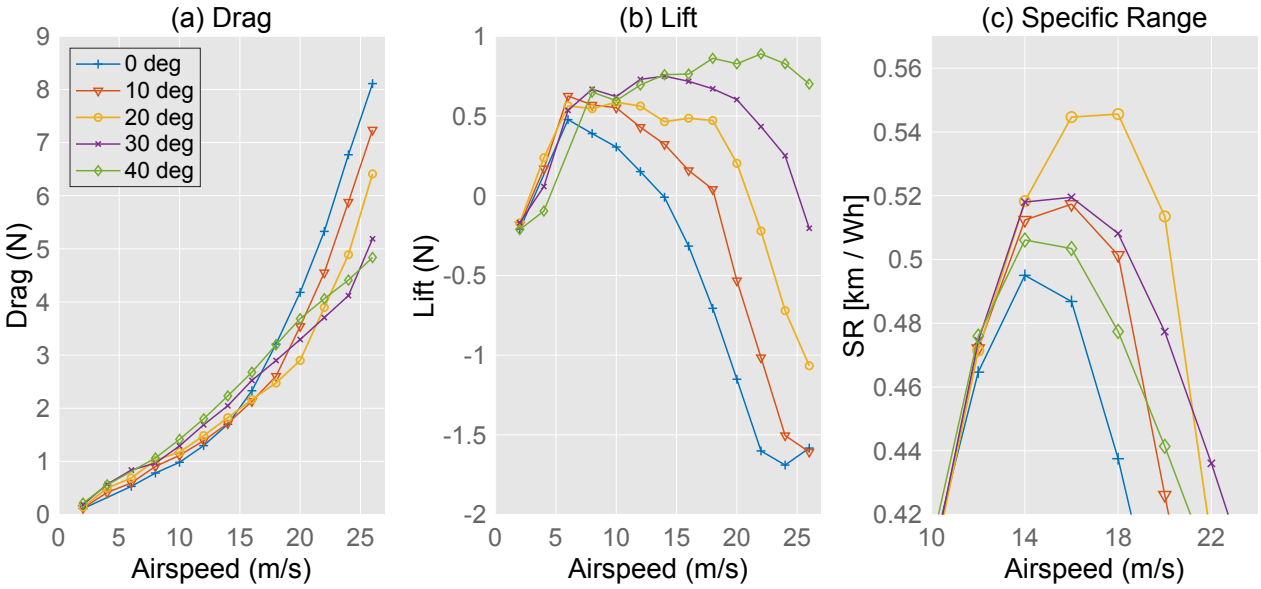

Figure 13: Comparison of airframe drag (a) and lift (b) forces, and UAV's Specific Range (c) in trimmed forward flight conditions for different rotor tilt angles.

in a standard configuration due to the smaller overlap between rotors, and the $\xi = 40°$ case still suffers from this effect in its offset configuration. Figure 16 shows the flow streamlines that intersect the rotor disks for the standard (a) and offset (b) configurations with a tilt of $\xi = 30°$ at an airspeed of 16 m/s which corresponds to the airspeed at which both cases reach their highest Specific Range. The front rotors' streamlines are coloured blue while the back rotors' are coloured orange. The Figure shows how the vertical offset between rotors significantly reduces the overlap between rotors and allows the back rotors to ingest undisturbed air in the offset case. The difference in behaviour between cases is also showcased in Figures 17 and 18, in which zones of high vorticity magnitude are drawn for two cases: tilt angle of 20° with an offset in the vertical separation and tilt angle of 30° with the standard vertical separation, both flying with an airspeed of 8 m s^{-1}. The changes in the airframe angle and the relative position of the propellers lead to drastic changes in their wake and their interaction.

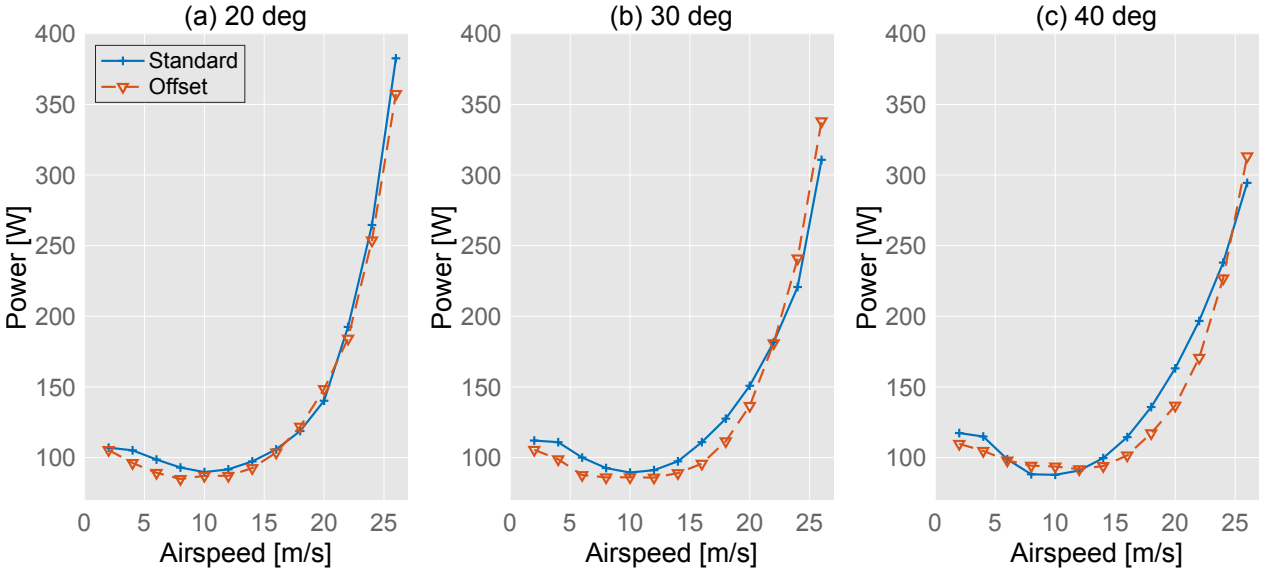

Figure 14: Comparison of the standard and offset configuration's total mechanical power for rotor tilt angles of $\xi = 20°$ (a), $\xi = 30°$ (b), and $\xi = 40°$ (c).

To conclude, the offset case with a tilt angle of $\xi = 30°$ showed an increase of 21.6% and 10.3% in maximum SR when compared to the standard non-tilted configuration and best standard tilted configuration ($\xi = 20°$) respec-

DOI: 10.13009/EUCASS2025-518

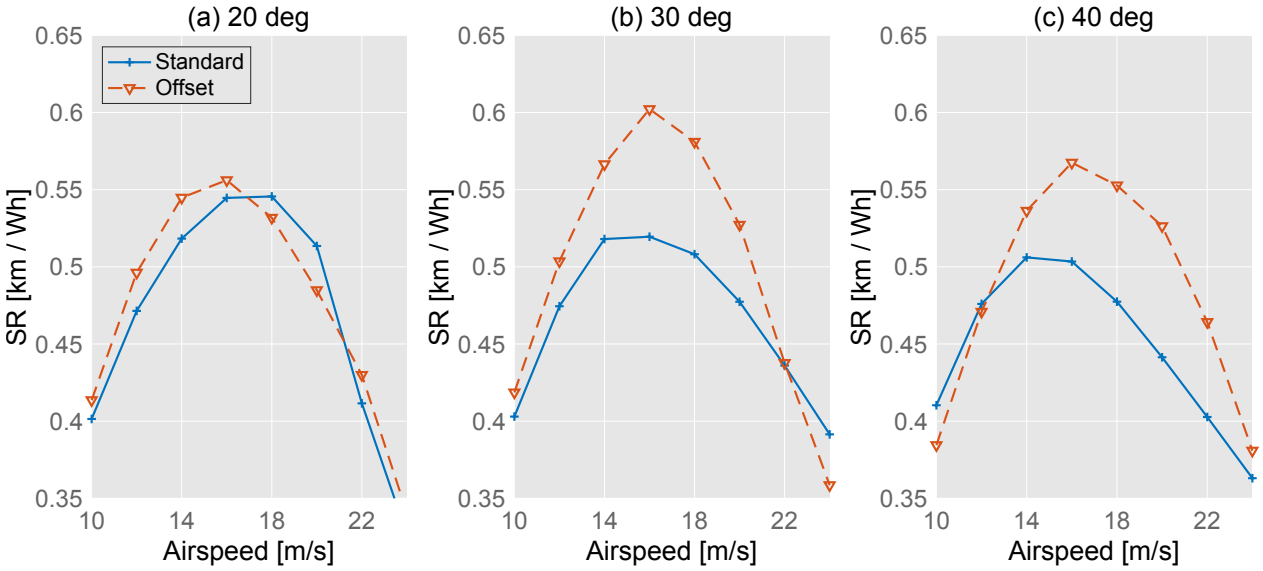

Figure 15: Comparison of the standard and offset configuration's Specific Range for rotor tilt angles of $\xi = 20°$ (a), $\xi = 30°$ (b), and $\xi = 40°$ (c).

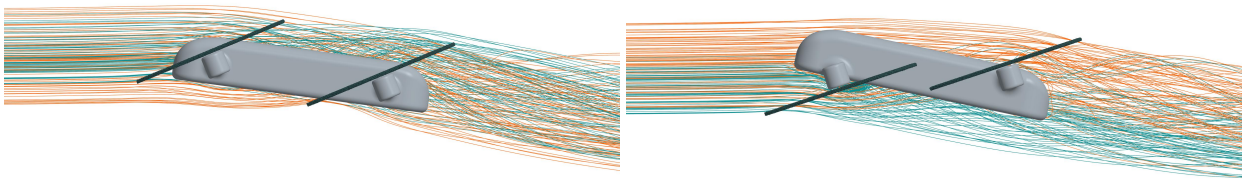

(a) Standard configuration

(b) Offset configuration

Figure 16: Two renders illustrating the flow streamlines that intersect the rotor disks for the standard and offset configurations with a tilt angle of $\xi = 30°$ at an airspeed of 16 m/s. The streamlines that pass through the front rotors are coloured blue while the ones that pass through the back rotors are coloured orange.

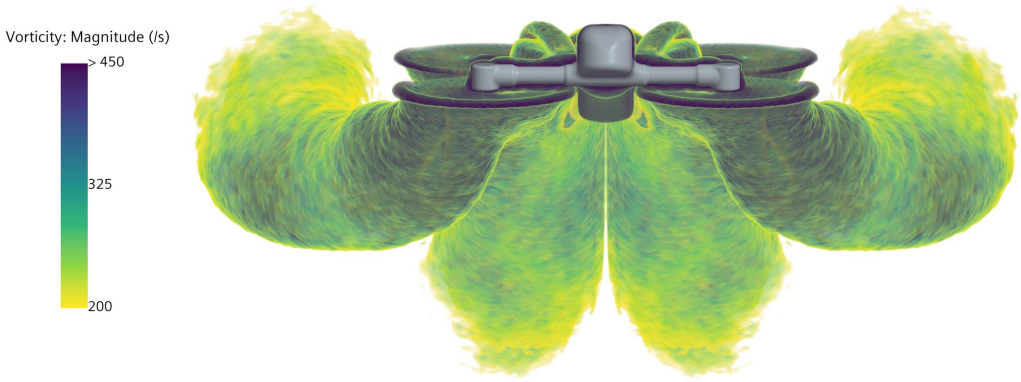

Figure 17: Render representing the regions of the flow in which the vorticity magnitude is above 200 $s^{-}1$ for the offset case with a tilt angle of 20° at an airspeed of 8 m/s.

tively, while the offset configuration with $\xi = 20°$ was able to reduce minimum power and thus, the UAV's maximum achievable endurance by a more modest 2.9% when compared to the lowest minimum power achieved by the standard configuration ($\xi = 0°$). The best performance values bar power at 26 m/s were achieved with the offset configuration.

DOI: 10.13009/EUCASS2025-518

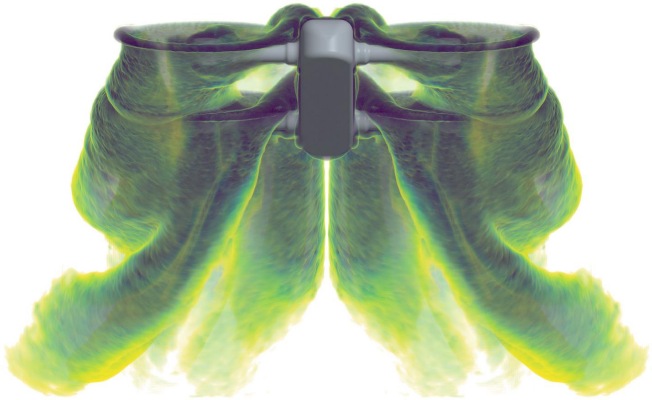

Figure 18: Render representing the regions of the flow in which the vorticity magnitude is above $200\,s^{-}1$ for the standard case with a tilt angle of 30° at an airspeed of 8 m/s. The colours represent the same as in Figure 17.

8. Computational cost of the analysis

The simulations required an average of 280 Intel Xeon 8480 core hours each. A total of 108 different simulations were carried out, and the entirety of the simulation results presented in the current work required approximately 3×10^4 Intel Xeon 8480 core hours in total. Using 7 nodes and 784 CPU cores on the UPV's Sirius Computing Cluster, the entire simulation campaign was completed in just under 2 days.

9. Conclusions and final remarks

In the current work, a novel and affordable steady-state Computational Fluid Dynamics simulation approach was applied to quantify the effects of alternative rotor configuration on the forward flight performance of a small-scale quad-rotor UAV. A preliminary analysis was carried out to determine the potential benefits and drawbacks of tilting the rotors and inform the designs chosen for the comparative analysis. As a result, three types of configurations were chosen and subsequently evaluated: The first consisted of a standard non-tilted configuration, in the second the rotors were simply tilted by different angles, while the last was a configuration in which the back rotors were placed higher than the front ones.

The standard non-tilted configuration's simulation results were then used to estimate the UAV's electrical power consumption. The results were then compared to experimental measurements. The results showed a good prediction of trends and good agreement for moderate airspeeds. However, certain discrepancies were observed, notably at high speeds. The authors of the current work will focus their future efforts to investigate the said discrepancies.

The performance analysis revealed several key results. Firstly, it was found that the overall best performance was not achieved by the cases with the highest tilt angle. The findings showed that there exists a point at which increasing the tilt angle is no longer beneficial for all operating points, as it caused an increase in aerodynamic forces on the airframe at low to moderate airspeeds, and increased rotor wake interactions. Very large tilt angles were found to be most optimal at reducing power requirements at very high airspeeds. Secondly, the introduction of a vertical offset between rotors was showed to enhance the performance gains of tilted configurations through reduced rotor wake interactions. In fact, through simple changes to the rotor configurations, maximum range was increased by up to 21.6% and minimum power was decreased by up to 2.9% when compared to the baseline case.

10. Acknowledgments

The results of this work are part of project AURORA, Grant PID2023-150573OB-I00 funded by MICIU/AEI/10.13039 /501100011033 and by ERDF/EU. The authors are grateful for the computational resources provided by the Sirius Scientific Computing Cluster of the Universitat Politecnica de Valencia, and additionally wish to thank Haoyun Jerry, Tang and Mark W. Mueller for providing the PairTilt UAV's assembly and facilitating the study carried out in the current work.

DOI: 10.13009/EUCASS2025-518

References

[1] Delair UX11 specifications. https://delair.aero/wp-content/uploads/2023/04/Datasheet_UX11_2022-28-04.pdf.

[2] Mavic 4 Pro specifications. https://www.dji.com/es/mavic-4-pro/specs.

[3] Sirius scientific computing cluster web-page.

[4] Patricia Ventura Diaz and Steven Yoon. High-fidelity computational aerodynamics of multi-rotor unmanned aerial vehicles. In *2018 AIAA Aerospace Sciences Meeting*.

[5] Luis Miguel García-Cuevas González, Jorge García-Tiscar, Pau Varela Martínez, and Brendan Mullen. Numerical analysis of quad-rotor aerodynamic and aeroacoustic performance with automated trimming algorithm. Submitted for review to Aerospace Science and Technology the 26th of May of 2025. Preprint available in https://www.researchgate.net, 2025.

[6] Derya Kaya. *Estimation of Aerodynamic Loads of a Propeller through Improved Blade Element and Momentum Theory and Propeller Design Optimization*. PhD thesis, 06 2021.

[7] D. Langkamp. *Quadrotor Flight Performance*. PhD thesis, TheUniversity of Manchester, 2012.

[8] J. Gordon Leishman. *Principles of Helicopter Aerodynamics*. Cambridge Aerospace Series. Cambridge University Press, 2016.

[9] F. R. Menter. Two-equation eddy-viscosity turbulence models for engineering applications. *AIAA Journal*, 32(8):1598–1605, 1994.

[10] J. Seddon. *Basic Helicopter Aerodyamics*. BPS Professional Books, 1990.

[11] Siemens Digital Industries Software. Simcenter STAR-CCM+, version 18.06.007-r8.

[12] Jerry Tang, Karan P. Jain, and Mark W. Mueller. Quartm: A quadcopter with unactuated rotor tilting mechanism capable of faster, more agile, and more efficient flight. *Frontiers in Robotics and AI*, Volume 9 - 2022, 2022.

[13] Jerry Tang and Mark Mueller. Pairtilt: Design and control of an active tilt-rotor quadcopter for improved efficiency and agility. *Advanced Intelligent Systems*, 02 2025.

[14] Haotian Zhang, Shaochang Tan, Ziming Song, and Quan Quan. Performance evaluation and design method of lifting-wing multicopters. *IEEE/ASME Transactions on Mechatronics*, PP:1–1, 06 2021.

A. Estimating the UAV's total mechanical power using momentum theory

The following computations are carried out following classic momentum theory for helicopter as describes by J. Gordon Leishman[8] and J.Seddon.[10] First the induced velocity and ideal power in hover are computed using Equations 11 and 12:

$$v_{i_o} = \left[\frac{W/4}{2 \cdot \rho \cdot S}\right]^{1/2}, \tag{11}$$

$$P_{i_o} = 2 \cdot \rho \cdot S \cdot v_{i_o}^3, \tag{12}$$

where $S = \pi R_p^2$ is one rotor disk's area. Next, the non-dimensional velocity is computed as:

$$\overline{V} = V/v_{i_o}. \tag{13}$$

Following this, rotors' and airframe's parasitic power, and induced power can be computed and summed to obtain the total mechanical power. For each rotor, the parasitic power is computed as:

$$P_{\text{pr}} = \frac{1}{\eta} P_{i_o} \overline{P_o} \left[1 + 5\left(\frac{v_{i_o}}{\Omega R_p}\right)^2 \overline{V}^2\right], \tag{14}$$

where

DOI: 10.13009/EUCASS2025-518

$$\overline{P_o} = \frac{\sigma \overline{c_d}}{16} \frac{1}{(v_{i_o}/\Omega R_p)^3}, \tag{15}$$

and $\sigma = (b.c.R_p)/S$ is the rotor's solidity, $b = 2$ is its number of blades, $c = 0.175R_p$ is its blades' mean chord length, $\overline{c_d} = 0.04$ the blade's airfoil's drag coefficient taken for an angle of attack of 8° and a Reynolds number of 80 000, Ω the rotor's angular velocity, and $\eta = 0.6$ is the rotor's estimated aerodynamic efficiency. The angular rate is considered equal for all four rotors, and considered proportional to the square root of the total thrust of the UAV. The relationship between total thrust and the rotors' angular rate is estimated as:

$$\Omega = [\frac{T}{4K_T}]^{1/2}, \tag{16}$$

where $K_T = 7.64E - 6$ is the factor between the 8045 rotor's thrust and the square of its angular rate. This value is taken from J.Tang and M.Mueller's work.[13] The airframe's parasitic power is computed as:

$$P_{pf} = V \cdot D, \tag{17}$$

and induced power is computed using the following equation:

$$P_{\text{ind}} = \frac{1}{\eta} P_{i_o} \left[\left[1 + \frac{1}{4} \overline{V}^4 \right]^{1/2} - \frac{1}{2} \overline{V}^2 \right]^{1/2}. \tag{18}$$

Finally, the different contributions are summed to obtain the total power:

$$P_{\text{tot}} = P_{pf} + 4 \cdot (P_{\text{pr}} + P_{\text{ind}}). \tag{19}$$

B. Additional tables

Table 1: Fit coefficients

Coefficient	Value
a	1.999×10^{-7}
b	-9.146×10^{-6}
c	5.077×10^{-3}
d	1.485×10^{-1}
a_0	3.448×10^{-2}
a_1	-3.563×10^{-2}
b_1	1.233×10^{-1}
w	3.971×10^{-2}

Table 2: Trim algorithm's Proportional-Integral coefficients.

Loop	K_P	K_I (iteration^{-1})	Units
1	1	10	rad s^{-1} N^{-1}
2	0.002	0.015	rad N^{-1}
3	5	30	rad s^{-1} N^{-1} m^{-1}